Crystal-Amorphous and Crystal-Crystal Phase Transformations via Virtual Melting

Valery I. Levitas

Texas Tech University, Center for Mechanochemistry and Synthesis of New Materials, Lubbock, Texas 79409, USA

(Received 27 August 2004; published 8 August 2005)

A new mechanism of crystal (c)–amorphous (a) and c-c phase transformations (PTs) and internal stress relaxation via virtual melting (VM) induced by internal stresses was justified thermodynamically and kinetically. VM removes interface friction, reduces kinetic barrier, increases atomic mobility, and can reduce thermodynamic melting temperature. We combine VM and nonequilibrium PT diagrams to develop new scenarios of c-a and c-c PTs. Results are applied for a new interpretation of c-c and c-a PT mechanisms in ice Ih and are also applicable for other materials.

DOI: 10.1103/PhysRevLett.95.075701 PACS numbers: 64.70.Kb, 64.60.−i, 68.35.Rh

Pressure- and temperature-induced c-a phase transformations (PTs) were considered (e.g., for ice, quartz, high albeite, $Cd_{43}Sb_{57}$, and jadeite [1–5]) as a low temperature *analog* of melting along the continuation of melting lines in a pressure-temperature (p-θ) phase diagram (Fig. 1). Alternatively, amorphization was related to the loss of mechanical stability of the crystal lattice [2,4,6–9]. However, some contradictions were found concerning metastable melting [6–9] and instability [2,7,8] hypotheses. In this Letter, we justify, thermodynamically and kinetically, new mechanisms of c-a and c-c PTs and internal stress relaxation via virtual melting (VM) as well as via VM induced by internal stresses. The *virtual melt* represents a short-lived melt (transitional state) of the parent phase below the thermodynamic melting temperature. Material melts when the p-θ loading trajectory crosses the low temperature continuation of nonequilibrium melting line (Fig. 1) and when c-c PT is suppressed due to elastic energy, interface friction, and kinetic barriers. The virtual melt is stable with respect to parent c phase but unstable with respect to product (c or a) phase, which is why it solidifies immediately to the $2c$ phase (above the glass transition temperature, θ_g) or to the $2a$ phase (below θ_g). Internal stress-induced VM [Fig. 2(c)] is thermodynamically promoted by the energy of internal stresses caused by c-c PT, which is why it occurs even before crossing the nonequilibrium melting line (Fig. 1). VM removes the interface friction, reduces the kinetic barrier, increases the atomic mobility, and is able to reduce the thermodynamic melting temperature. These theoretical predictions allowed us to resolve some known contradictions [6–9] and interpret some experimental data that could not be interpreted using existing approaches.

Nonequilibrium PT diagrams.—We consider materials with the equilibrium p-θ diagram similar to that shown in Fig. 1 and with a large volumetric transformation strain, $\varepsilon_0 > 0.1$. However, for analysis of actual PTs one needs to determine nonequilibrium PT diagrams (Fig. 1) and parameters that affect them [7]. The thermodynamic net driving force, $F_{1\to2}$, for nucleation of phase 2 in the volume V bounded by the surface Σ, under external pressure p, is [10]

$$F_{1\to2} = \Delta g_V V - \Delta\Gamma\Sigma;$$
$$\Delta g_V := p\varepsilon_0 - \Delta g_{1\to2}(\theta) - g^e + g^d - K, \tag{1}$$

where $\Delta g_{1\to2}$ is the change in the thermal part of the Gibbs energy, g^e and g^d are the energies of internal stresses caused by ε_0 and nucleating defect, correspondingly, K is the athermal dissipation related to interface friction and caused by a long range stress field of various defects, and $\Delta\Gamma$ is the change in interface energy. The change in elastic moduli is neglected for compactness. For large ε_0 and elastic energy g^e, a nucleus is a penny-shaped ellipsoid

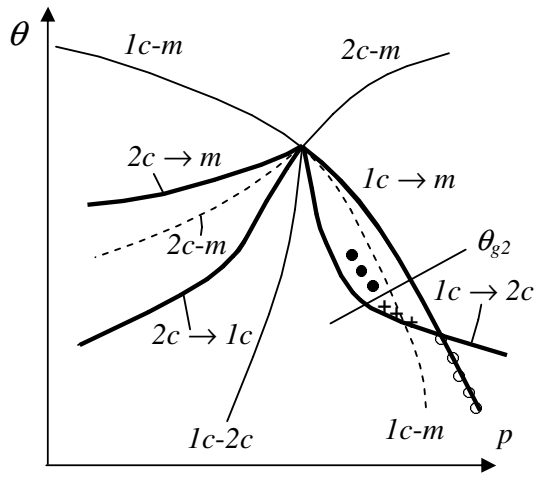

FIG. 1. Equilibrium and nonequilibrium PT pressure (p)-temperature (θ) diagrams. Solid lines ($1c$-m, $2c$-m, $1c$-$2c$) are the phase equilibrium lines. Dashed lines are the metastable continuation of $1c$-m and $2c$-m lines. Bold lines are calculated lines for the initiation of PTs ($1c \to 2c$, $2c \to 1c$, $1c \to m$, $2c \to m$). The straight line is the glass formation temperature θ_{g2}. PTs during compression: ●, $1c \to$ internal stress-induced VM $\to 2c$ PT around $2c$ nuclei (above θ_{g2}); +, $1c \to$ internal stress-induced VM $\to 2a$ PT around $2c$ nuclei (below θ_{g2}); both ● and + PT start before reaching equilibrium $1c$-m or nonequilibrium $1c \to m$ melting lines; ○, $1c \to$ VM $\to 2a$ PT.

[10–13]; see Fig. 2. The diffusion controlled nucleation rate is $N \sim \exp[-(E_{sd} + G_{cr})/k\theta]$, where E_{sd} is the activation energy of self-diffusion, $G_{cr} \sim \Delta\Gamma^3/\Delta g_V^4$ the energy of critical penny-shaped nucleus [11], and k the Boltzmann constant. For an observable nucleation rate it is usually assumed $(E_{sd} + G_{cr})/k\theta = 40$–$80$ [11]; this condition is used to determine each line on the nonequilibrium PT diagrams (Fig. 1). For c–melt (m) PT, the same expressions for $F_{1\to2}$, G_{cr}, and N are valid; however, $K = 0$, because the hydrostatic medium does not interact with the stress field of crystal defects [12], and g_m^e is negligible [12,13]. Thus, actual nonequilibrium PT lines are significantly shifted with respect to the phase equilibrium lines due to (a) thermodynamic barrier $g^e - g^d$, (b) interface friction K, and (c) kinetic barrier $G_{cr} + E_{sd}$ (Fig. 1).

In contrast to previous theoretical studies of c-a and high pressure c-c PT [2,3,5,7–9], we include athermal friction K [10] and treat comprehensively the elastic energy. It follows from the definition of a nonequilibrium PT diagram that if the p-θ loading trajectory crosses some nonequilibrium PT line, corresponding PT *must* occur. This is in contrast to the equilibrium PT diagram, in particular, for melting (dashed lines in Fig. 1), which is usually used for analysis of amorphization [1,5–9]. The use of nonequilibrium melting lines explains why amorphization lines may be located above the dashed lines in some experiments (Fig. 1).

Virtual melting.—Let us consider the loading path that crosses the melting line $1c \to m$ in the stability region of phase 2 (Fig. 1). If melting occurs far from the $2c$-m line (as in Fig. 1), the melt is unstable with respect to phase 2, and fast solidification will occur immediately after melting. Above θ_g solidification occurs to the $2c$ phase, while below θ_g amorphization occurs to the $2a$ phase [Figs. 2(a) and 2(b)]. A short-lived unstable (with respect to the product c or a phase) melt (transitional state) is called the *virtual melt.* This is in contrast to a long-lived metastable melt existing close to the $2c$-m line where solidification is kinetically suppressed. Thus, VM is a new mechanism for amorphization and c-c PT. Usually, a crystal is considered to directly vitrify into an amorphous state [1–5], which results in some contradictions [7–9]. Consideration of VM as a separate process followed by solidification below θ_g reduces the solid-state amorphization to solidification of undercooled liquid after quenching with an infinite cooling rate to the temperature at which $1c \to$ VM PT occurs. This allows the resolution of some contradictions [7–9]: (a) The sign of heat for melting and amorphization is different, because heat of amorphization includes heat of melting $1c \to$ VM and solidification VM $\to 2a$. (b) For amorphization along the line $1c \to m$, in experiment the short range order structure corresponds to phase $2c$ (rather than $1c$). This is because the amorphous phase is quenched from the VM in the region of the stability of phase 2, and the atomic mobility in liquid is much higher than in solid. (c) The structure of pressure-induced amorphous phase and amorphous phase quenched from a melt can be different (e.g., for ice [9]), because VM may have a different structure than the equilibrium melt. Also, since the VM corresponds to quenching with an infinite cooling rate, less time is available to change the structure.

Internal stress-induced VM.—For a coherent $2c$ penny-shaped nucleus with semiaxes b and r, $n = b/r \ll 1$ [Fig. 2(c)], $g_c^e \simeq \mu\varepsilon_0^2(1+\nu)/[8(1-\nu)] > 0$, where μ is the shear modulus and ν is the Poisson's ratio [12]. Let a coherent $2c$ nucleus grow to sizes b_c and r_c and plastic relaxation be suppressed. We estimate the possibility of melt nucleation around the $2c$ nucleus; let the external melt surface be also ellipsoidal with the semiaxes b_m and r_m, $n_m = b_m/r_m \ll 1$ [Fig. 2(c)]. The net driving force for melt nucleation is derived in the form

$$F_{1\to m} = F_e + [p\varepsilon_0^m - \Delta g_{1-m}(\theta)]4\pi(r_m^2 b_m - r_c^2 b_c)/3 - 2\pi\Gamma_{1-m}(r_m^2 - r_c^2), \quad (2)$$

where $F_e = g_c^e 4\pi r_c^2 b_c/3 - 2\pi r_c^2(\Gamma_{1-m} + \Gamma_{2-m} - \Gamma_{1-2})$ and Δg_{1-m} is the change in the thermal part of the Gibbs energy during melting. Since the $2c$ nucleus loses its coherency, its elastic energy g_c^e releases, increasing the driving force for $1c$-m PT. If $F_e > 0$, there exists a unique situation for nucleation: the driving force for melting is positive even for infinitesimal m volume; i.e., *barrierless*

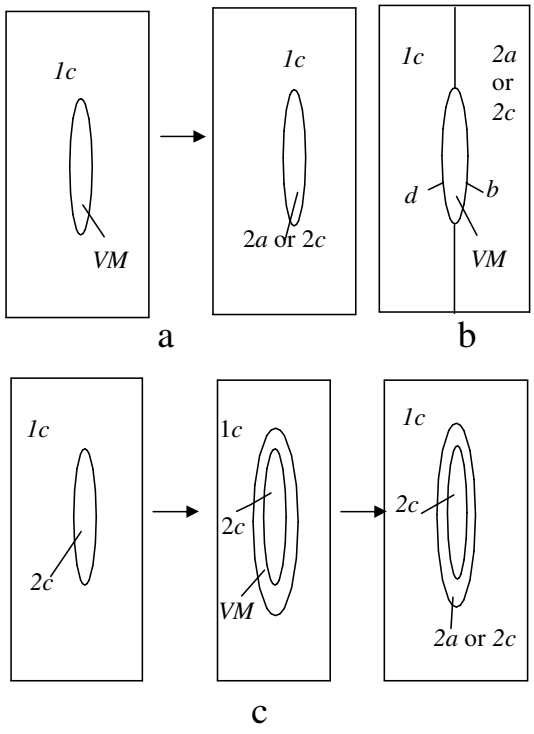

FIG. 2. Solid-solid PTs via virtual melting. (a) Nucleation of VM inside the $1c$ phase followed by solidification to the $2c$ or $2a$ phase; (b) growth of $2c$ or $2a$ phase via VM; after solidification, the interface moves from position b to d; (c) PT $1c \to$ internal stress-induced VM $\to 2a$ (or $2c$) around the $2c$ nucleus.

melting induced by the release of internal stresses in an enclosed 2c nucleus takes place. The condition for barrierless melting, $F_e > 0$, is $g_c^e > 1.5(\Gamma_{1-m} + \Gamma_{2-m} - \Gamma_{1-2})/b_c$. Taking $\Gamma_{1-m} = \Gamma_{2-m} \gg \Gamma_{1-2}$, one obtains the minimal size of $2c$ nucleus, $b_{c0} = 3\Gamma_{1-m}/g_c^e$. Estimates for b_{c0} for PTs in ice (Table I) give realistic numbers. Even if $p\varepsilon_0^m < \Delta g_{1-m}$, i.e., when there is no stimulus for the usual melting, melt induced by internal stresses can nucleate if $F_e > 0$ [because for small melt nucleus $F_{1\to m} \geq 0$ in Eq. (2)]. The size $b_m = b_c$ of melt nucleus is determined from the condition $F_{1\to m} \to \max$; the size r_m can be found from the condition $F_{1\to m} = 0$. Thus, internal stresses not only remove the kinetic barrier, but also can lower the thermodynamic melting line (Figs. 1 and 3). Energy g_c^e reduces the melting pressure by $\Delta p = \frac{g_c^e}{\varepsilon_0^m(um-1)}(1 - \frac{u+1}{2y})$ with $m = b_m/b_c$, $u = r_m^2/r_c^2$, and $y = b_c/b_{c0}$ (obtained from the condition $F_{1\to m} = 0$). Using data from Table I for Ih → IX PT in ice, $y = 2$, $m = 1$, $u = 1.2$, we obtain $\Delta p = 0.38$ GPa, which exceeds maximum deviation between the experimental amorphization line and the calculated melting line at $\theta = 150$ K [6,9] (Fig. 3). The experimental fact that for some materials (e.g., for ice [6]) amorphization starts below the melting pressure was used as one of the main contradictions of the metastable melting hypothesis [6–9]. The shift in the thermodynamic melting line due to internal stresses resolves this seeming contradiction. Our estimates also show that if VM is impossible, then the fulfillment of a condition similar to $F_e > 0$ can promote direct amorphization around the $2c$ nucleus (internal stress-induced amorphization), since amorphization releases the major part of g^e. The thermodynamic and kinetic advantage of amorphization around the $2c$ nucleus (direct or via VM) in comparison with direct $1c \to 2a$ PT explains why the mixture of small size crystalline nuclei and an amorphous phase is observed in experiments [6,7].

Consider a large number of $2c$ nuclei that cause $1c \to$ VM $\to 2a$ PT, after which growth is limited. Since in the equation for the nucleation rate of $2a$ phase $N \sim \exp[-(E_{\rm sd}^m + G_{\rm cr})/k\theta]$, $G_{\rm cr}$ is negative (barrierless nucleation), and $E_{\rm sd}^m$ for melt is smaller than $E_{\rm sd}^s$ for $1c$, it explains why activation energy for amorphization is smaller than $E_{\rm sd}^s$, e.g., in experiments on $Zn_{43}Sb_{57}$ [5].

Let us consider the growth of incoherent $2c$ and $2a$ nuclei after VM, in the region where both direct solid-solid PT and VM are possible (Fig. 1). For solid-solid PT, the interface velocity $v \sim \exp(-E_a/k\theta)[1 - \exp(-F_{1\to 2}^s/k\theta)]$, where E_a is the activation energy [11]. For atom by atom growth, $E_a \simeq E_{\rm sd}^s$; however, adding a single atom to a flat interface significantly increases g_e and reduces $F_{1\to 2}$ [11]. Thus, nucleation of kink or ledge may be necessary for growth, which requires additional energy E_n, and then [11] $E_a = E_{\rm sd}^s + E_n$. If the solid-solid interface moves via nucleation and solidification of VM [Fig. 2(b)], then $v \sim \exp[-(E_{\rm sd}^m + E_n^m)/k\theta][1 - \exp(-F_{1\to 2}^m/k\theta)]$. The driving force for $1c \to 2c$ or $1c \to 2a$ PTs via VM $F_{1\to 2}^m > F_{1\to 2}^s$, because $F_{1\to 2}^m$ does not contain K and g^e is smaller. Indeed,

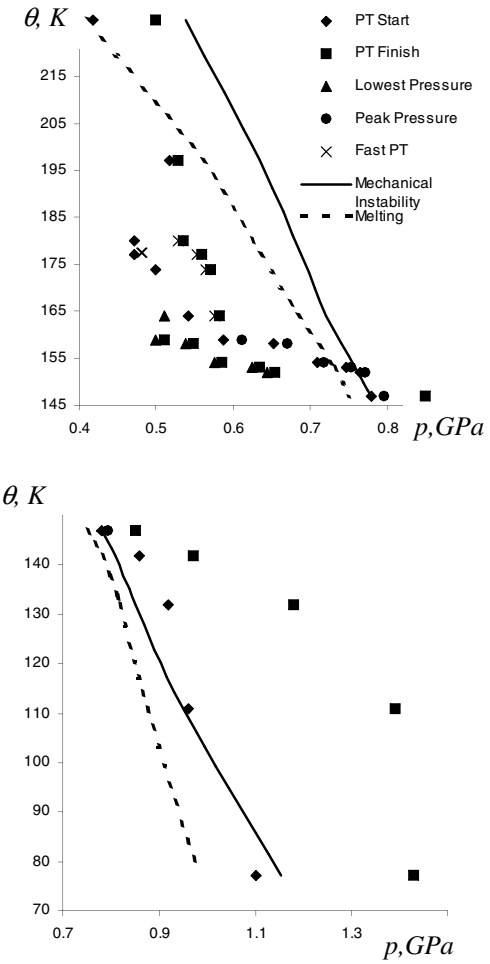

FIG. 3. PTs in ice Ih under compression. All symbols are points from the pressure-piston displacement curves from [6]. Dashed and solid lines are equilibrium melting and lattice instability curves from MD simulation in [9]. Results of our interpretation: 197–227 K: thermodynamic melting; 164–180 K: PT to ices V or IX or III; system instability at 164 K is caused by internal stress-induced VM; 152–159 K: Ih → IX → internal stress-induced VM → amorphous ice; below 150 K: Ih → VM → amorphous ice PT.

TABLE I. Calculated elastic energy, g_c^e, and minimal size of $2c$ nucleus, b_{c0}, necessary for barrierless internal stress-induced VM for PTs in ice. Γ_{1-m} is taken from [14], other material parameters are from [15].

PT	θ (K)	μ (GPa)	ν	ε_0	Γ_{1-m} (J/m^2)	g_c^3 (MJ/m^3)	b_{c0} (nm)
Ih → IX (or II)	160–180	3.5	0.32	0.2	0.028	34	2.47
Ih → XII	77	3.5	0.39	0.3	0.028	90	0.93

for solid state, the deviatoric stresses at the level of the macroscopic yield stress remain even for incoherent interface; also $E^m_{sd} < E^s_{sd}$. Energy of the critical m nucleus $E^m_n \sim \Delta\Gamma^3/\Delta g^4_V$ [10,11], where $\Delta\Gamma = \Gamma_{1-m} + \Gamma_{2-m} - \Gamma_{in}$, can be small or even negative (due to $\Delta\Gamma < 0$), thus $E^m_n < E_n$, and activation energy for growth is much smaller than E_{sd} in solids, like in experiments [5] on $Zn_{43}Sb_{57}$. Thus, in some cases propagation of solid-solid interfaces via VM is thermodynamically and kinetically favorable. Both nucleation and growth via VM: (a) reduce the elastic energy; (b) remove the athermal friction K; (c) increase the mobility of atoms; (d) reduce the activation energy for the formation of kink or ledge.

PTs in ice Ih.—The main conclusion of [6,9] is that above 160 K there is a thermodynamic metastable melting, while amorphization below 160 K is related to lattice instability. Here we suggest an alternative interpretation (Fig. 3) of the mechanisms of PT in Ih ice in [6], using the above theory. We demonstrate that the mechanisms of c-c and c-a PT via VM and internal stress-induced VM is consistent with the experimental data [6] in various temperature ranges, in contrast to interpretation in [6,9].

It was suggested for $160 < \theta < 190$ K that after thermodynamic melting homogeneous crystallization of ices V or IX or III occurs [6]. However, since the net PT is exothermic, there was no direct evidence of melting. At 180, 177, and 174 K, PT starts at lower pressure than at 197 K, and with a different slope. This cannot be thermodynamic melting, because pressure is smaller than the calculated melting pressure [9]. This also cannot be lattice instability, because the PT is slow (large slope dp/du, where u is the piston displacement proportional to change in a specimen volume [6]) and slope dp/du increases with the pressure; moreover, the lattice instability line is far from the PT line [9] (Fig. 3). Thus, direct $c \rightarrow c$ PT to phases V and III or IX can occur only.

At 164 K, system instability ($dp/du < 0$) was observed. This cannot be explained by lattice instability, because $dp/du > 0$ corresponding to slow phase growth (similar to that at 174–180 K) follows the system instability. Negative dp/du can be explained by *internal stress-induced* VM around the ice IX nuclei followed by solidification to the ice IX. This removes K and releases elastic energy utilized for further growth increment, i.e., leads to the burstlike PT.

For $150\ \text{K} < \theta < 160$ K, system instability was observed, which leads to complete PT. This cannot be explained by lattice instability because at $77 < \theta < 142$ K, for much higher pressure and much closer to calculated lattice instability line, $dp/du > 0$ was observed [6]. We propose that after ice IX nuclei appeared and when pressure reached some critical value (peak point), internal stress-induced VM occurs around the nuclei followed by amorphization.

Below 150 K, the amorphization mechanism cannot be related to lattice instability because there is no system instability and PT kinetics is slow. The amorphization pressure is significantly higher than the calculated [9] lattice instability pressure, showing contradiction in calculations [9] at low temperature. Amorphization mechanism via VM is consistent with the existing data (Fig. 3). Since there is no c-c PT promoting VM, melting does not start below equilibrium melting pressure and does not cause $dp/du < 0$.

In summary, we predicted that VM and internal stress-induced VM represent new mechanisms of c-c and c-a PTs, stress relaxation, removing athermal friction, increasing atomic mobility, decreasing a kinetic barrier, and reducing the thermodynamic melting temperature. VM mechanisms resolve a number of contradictions in the interpretation of experimental data in [6–9]. They are consistent with existing experimental data [1,5–8]. Current results significantly expand the VM idea suggested in [12] and its area of applicability. In addition to ice, VM is expected in the amorphization of α-quartz and coesite [4], polymet [8], Ge and Si [7,8], jadeite, $Zn_{43}Sb_{57}$ and $Cd_{43}Sb_{57}$ [4], BN, and graphite. These materials have an equilibrium p-θ diagram similar to that shown in Fig. 1 and their amorphization occurs near the extrapolated metastable melting line. Note that amorphization and consequently VM, e.g., in Si and Ge [7], occur at more than 1000 K below the thermodynamic melting temperature at the same pressure.

The support of NSF (CMS) is gratefully acknowledged.

[1] O. Mishima, L. D. Calvert, and E. Whalley, Nature (London) **310**, 393 (1984).
[2] W. L. Johnson, Prog. Mater. Sci. **30**, 81 (1986).
[3] P. Richet, Nature (London) **331**, 56 (1988).
[4] R. J. Hemley *et al.*, Nature (London) **334**, 52 (1988).
[5] E. G. Ponyatovsky and O. I. Barkalov, Mater. Sci. Rep. **8**, 147 (1992).
[6] O. Mishima, Nature (London) **384**, 546 (1996).
[7] V. V. Brazhkin and A. G. Lyapin, High Press. Res. **15**, 9 (1996); V. V. Brazhkin *et al.*, J. Non-Cryst. Solids **212**, 49 (1997).
[8] S. M. Sharma and S. K. Sikka, Prog. Mater. Sci. **40**, 1 (1996).
[9] J. S. Tse *et al.*, Nature (London) **400**, 647 (1999).
[10] G. B. Olson and M. Cohen, in *Dislocations in Solids*, edited by F. R. N. Nabarro (Elsevier, New York, 1986), Vol. 7, pp. 297–407; V. I. Levitas, Int. J. Plast. **16**, 805 (2000); V. I. Levitas *et al.*, Philos. Mag. A **82**, 429 (2002).
[11] D. A. Porter and K. E. Easterling, *Phase Transformation in Metals and Alloys* (Van Nostrand Reinhold, New York, 1992).
[12] V. I. Levitas *et al.*, Phys. Rev. Lett. **92**, 235702 (2004).
[13] T. Mura, *Micromechanics of Defects in Solids* (Martinus Nijhoff, Dordrecht, 1987).
[14] P. Taborek, Phys. Rev. B **32**, 5902 (1985).
[15] E. L. Gromnitskaya *et al.*, Phys. Rev. B **64**, 094205 (2001); R. E. Gagnon *et al.*, J. Chem. Phys. **92**, 1909 (1990).